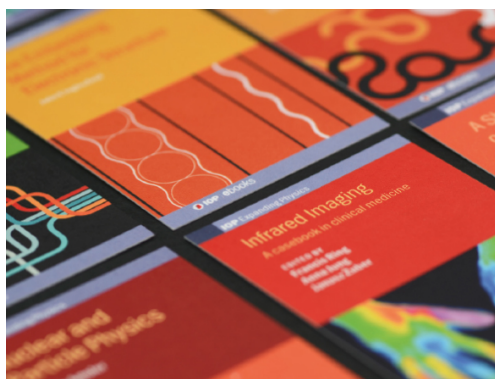


PAPER • OPEN ACCESS

## Operando XAFS investigation on the effect of ash deposition on three-way catalyst used in gasoline particulate filters and the effect of the manufacturing process on the catalytic activity

To cite this article: Monik Panchal *et al* 2021 *J. Phys.: Condens. Matter* **33** 284001

View the [article online](#) for updates and enhancements.













**IOP | ebooks™**

Bringing together innovative digital publishing with leading authors from the global scientific community.

Start exploring the collection—download the first chapter of every title for free.

# Operando XAFS investigation on the effect of ash deposition on three-way catalyst used in gasoline particulate filters and the effect of the manufacturing process on the catalytic activity

Monik Panchal<sup>1,2</sup> , June Callison<sup>2,6</sup> , Vainius Skukauskas<sup>2,3</sup> ,  
Diego Gianolio<sup>4</sup> , Giannantonio Cibi<sup>4</sup> , Andrew P E York<sup>5</sup> ,  
Manfred E Schuster<sup>5</sup> , Timothy I Hyde<sup>5</sup> , Paul Collier<sup>5</sup>,  
C Richard A Catlow<sup>1,2,6</sup>  and Emma K Gibson<sup>2,3,\*</sup> 

<sup>1</sup> Department of Chemistry, University College London, 20 Gordon Street, London WC1H 0AJ, United Kingdom

<sup>2</sup> UK Catalysis Hub, Research Complex at Harwell, Rutherford Appleton Laboratory, Harwell Science and Innovation Campus, Didcot, Oxon OX11 0FA, United Kingdom

<sup>3</sup> School of Chemistry, University of Glasgow, Glasgow G12 8QQ, Scotland, United Kingdom

<sup>4</sup> Diamond Light Source, Harwell Science & Innovation Campus, Oxfordshire OX11 0DE, United Kingdom

<sup>5</sup> Johnson Matthey Technology Centre, Blount's Court, Sonning Common, Reading, RG4 9NH, United Kingdom

<sup>6</sup> Cardiff Catalysis Institute, School of Chemistry, Cardiff University, Cardiff, United Kingdom

E-mail: [Emma.Gibson@glasgow.ac.uk](mailto:Emma.Gibson@glasgow.ac.uk)

Received 15 March 2021, revised 22 April 2021

Accepted for publication 4 May 2021

Published 4 June 2021



## Abstract


Platinum group metals such as palladium and rhodium based catalysts are currently being implemented in gasoline particulate filter (GPF) autoexhaust after treatment systems. However, little is known about how the trapped particulate matter, such as the incombustible ash, interacts with the catalyst and so may affect its performance. This *operando* study follows the evolution of the Pd found in two different model GPF systems: one containing ash components extracted from a GPF and another from a catalyst washcoat prior to adhesion onto the GPF. We show that the catalytic activity of the two systems vary when compared with a 0 g ash containing GPF. Compared to the 0 g ash sample the 20 g ash containing sample had a higher CO light off temperature, in addition, an oscillation profile for CO, CO<sub>2</sub> and O<sub>2</sub> was observed, which is speculated to be a combination of CO oxidation, C deposition via a Boudouard reaction and further partial oxidation of the deposited species to CO. During the ageing procedure the washcoat sample reduces NO at a lower temperature than the 0 g ash sample. However, post ageing the 0 g ash sample recovers and both samples reduce NO at 310 °C. In comparison, the 20 g ash GPF sample maintains a higher NO reduction temperature of 410 °C post ageing, implying that the combination of high temperature ageing and presence of ash has an irreversible negative effect on catalyst performance.

\* Author to whom any correspondence should be addressed.



Original content from this work may be used under the terms of the [Creative Commons Attribution 4.0 licence](https://creativecommons.org/licenses/by/4.0/). Any further distribution of this work must maintain attribution to the author(s) and the title of the work, journal citation and DOI.

Keywords: operando, x-ray absorption fine structure, gasoline particulate filter, three-way catalyst

 Supplementary material for this article is available [online](#)

(Some figures may appear in colour only in the online journal)

## 1. Introduction

The surge in the use of light-duty vehicles transport has resulted in increased air pollution through the combustion of fuels. In the UK since the early 2000s, 86% of commuters use cars, vans or motorcycles as their primary form of transport [1]. Sustainable fuel sources such as pure-electric and fuel cell powered systems have the potential to produce transport that emits near-zero tailpipe gases and particles. Though more sustainably powered vehicles have been commissioned, the technologies and infrastructure needed are still in their infancy for mass market adoption by consumers and thus internal combustion engine (ICE) powered vehicles will still be needed for several years [2–5]. Since the 1970s, emission standards and emission limits to air pollutants have led to the control of pollution levels in the short-term. These regulations are tightened every 4 to 10 years thus reducing the maximum emission limits, resulting in automotive companies searching for solutions to meet these ever-tightening standards [6, 7].

Common air pollutants generated by ICE, which have been regulated in the US and EU include: nitrogen oxides ( $\text{NO}_x$ ), unburnt hydrocarbons (HC), volatile-organic compounds, carbon monoxide (CO) and particulate matter (PM) [8]. Around, 86% of newly registered vehicles in the UK in 2019 use gasoline or diesel engines, with, studies showing these are a major contributor to PM emissions in urban areas [9–11]. Diesel vehicles are subject to emission controls towards PM emission number and mass. However, due to the mechanism of fuel injection in traditional port fuel injection gasoline engines, these engines result in a relatively low level of PM emissions [9, 12]. However, the recent market shift towards more fuel-efficient gasoline direct injection (GDI) engines, has consequently led to a change in the emission profile from gasoline vehicles [9, 12], —specifically, an increase in the mass and the number of smaller PM emission [13].

PM emissions can be divided into three sizes: coarse particles (diameter 2.5 to 10  $\mu\text{m}$ ,  $\text{PM}_{10}$ ), fine particles (0.1 to 2.5  $\mu\text{m}$ ,  $\text{PM}_{2.5}$ ) and ultra-fine particles (UFP) (less than 0.1  $\mu\text{m}$ ) [14]. As well as having an effect on the weather, climate and outdoor visibility, these sub-micron sized particles are inhalable and contribute to cardio-vascular and pulmonary related deaths [15, 16].

The toxicity effects of PM emissions can vary depending on their chemical composition, which can differ due to the emitter's fuel, lubrication oils, engine composition etc [17]. PMs are composed of a soot component (carbonaceous material from fuel combustion), and an ash component which consists of incombustible inorganic material, produced through the decomposition of engine additives (e.g. Fe, Ni, Cu,

Cr, Sn), oil lubrication, anti-wear additives and engine wear (e.g. Zn, Ca, Mg, Zn, Ti), normally in the form of metal sulphates, phosphates and oxides [18–21].

Gasoline particulate filters (GPFs), also known as ‘four-way catalytic convertors’, are a relatively novel automotive after treatment solution used in newer GDI engines. The system utilises a ‘three-way catalyst’ (TWC) to convert CO,  $\text{NO}_x$  and unburnt HC using a catalyst based on precious metal (Pt, Pd, Rh) supported over a mixed oxide ( $\text{CeZrO}_4$ ,  $\text{Al}_2\text{O}_3$ ). The catalyst is applied onto a honeycomb monolith, usually made of synthetic cordierite ceramic, which also traps PM emissions simultaneously [22].

PM components build up during operational filtration, which may result in blocked pores within the structure which in turn may affect the GPF operation conditions. Though most soot components are removed during operation through combustion using  $\text{O}_2$  and/or  $\text{NO}_2$  (passive regeneration), some incombustible materials such as ash are more difficult to remove through active regeneration strategies [23]. Therefore, due to their inability to be readily removed, these inorganic components are in proximity to the catalyst for longer times. The ash components from lubrication oils have been shown to have an impact on catalytic performance within diesel particulate filters; however, very little is known of their potential impact on a TWC system [24]. Over the lifespan of the GPF, the system may experience excursion temperatures around 1000 °C [25, 26]. With this in mind, it is important to understand how the catalytic system activity changes both on the incorporation of ash components and at these extremely high temperatures.

Several previous studies have used synchrotron based x-ray techniques, especially x-ray absorption fine structure (XAFS) to analyse TWC, enabling an understanding of the changes in the active metal species under different operation conditions [27–29]. A more recent study using operando x-ray absorption near edge structure (XANES) analysis on a GPF system, with and without ash loading and with ageing treatments suggested that light-off temperatures for CO, HC and  $\text{NO}_x$  increase with the loading. However, no XANES data were reported above light-off temperatures, i.e. above 300 °C and no data given on the catalytic activity of the washcoat prior to incorporation onto the monolith [30].

To understand these key effects of high temperatures on the ash loaded GPF TWC system, and on the effect that the manufacturing of the GPF plays on the performance of the catalyst, here we investigate an industrial GPF model catalyst based on a PdRh/CeZrO<sub>2</sub>/Al<sub>2</sub>O<sub>3</sub> catalyst. The effect of the manufacturing process on the catalyst activity was evaluated through the comparison of the catalytic activity of the

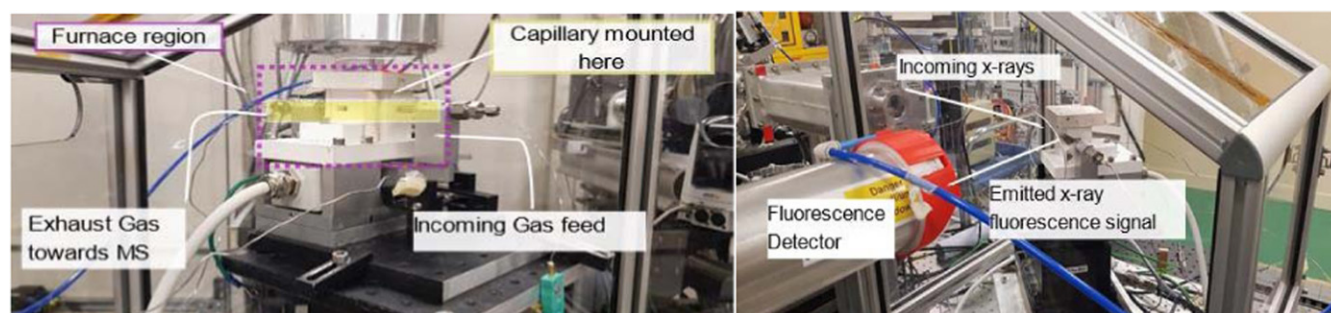


**Figure 1.** Annotated images of the capillary microreactor used for experiments on B18 at Diamond Light Source, showing the position of the capillary as gas feeds (Left) and the direction of the incoming beam and fluorescence detector position (Right).

fresh washcoat with a sample extracted from a GPF with no ash deposition (0 g GPF). The effect of ash on the system was achieved through comparing a heavily ash loaded sample (20 g l<sup>-1</sup>) acquired from a GPF monolith with the 0 g ash GPF sample. For the first time an *operando* XAFS study of the Pd *K*-edge has been performed for an ash loaded GPF sample subjected to high temperatures which may be observed during GPF operation (up to 1000 °C). In this study we have observed changes in the Pd of the 20 g l<sup>-1</sup> ash sample and the fresh washcoat catalyst during working conditions, by flowing a model gas mixture representative of exhaust gases and heating the catalyst to these extreme temperatures. Coupled with mass spectrometry, the CO oxidation, NO reduction and propane consumption profiles were followed and compared with the profile of a sample extracted from the 0 g ash GPF sample, in order to determine the role of the ash on the activity of the catalyst and the effect the GPF production plays on the activity of the initial catalyst formulation

## 2. Experimental section

### 2.1. Sample preparation

GPF samples were provided by Johnson Matthey plc. The Pd and Rh loading was at less than 1% wt on a CeZrO<sub>2</sub> support.

Ash was loaded onto the system using a DPG rig which uses diesel combustion to produce model PM. The GPF was weighed at 250 °C, followed by the addition of soot and ash (3:2 ratio) at 186 kg h<sup>-1</sup>. Soot was then removed through oxidation at 600 °C for 3 h under air. The GPF was then reweighed to determine the ash loading. This process was then repeated until the desired weight was achieved. Ash components were made through doping the diesel with Zinc dialkyldithiophosphates (ZDDP, 4 g l<sup>-1</sup>) and calcium sulphonate (4 g l<sup>-1</sup>), which is then co-combusted at 1 kg h<sup>-1</sup> through the DPG.

Three experimental samples were studied. Prior to experiment, the catalyst and ash species were extracted from the 20 g l<sup>-1</sup> GPF monolith through a process of grinding and sieving fragments of sample. The 0 g ash sample was likewise scraped from a GPF monolith, having not been treated in the DPG rig. A separate sample of catalyst washcoat (not applied to the GPF monolith) was acquired from a washcoat

slurry which was dried at 140 °C to remove solvent, affording a yellow powder.

### 2.2. XAS measurements

Operando XAFS experiments at the Pd *K*-edge on the 20 g ash GPF and washcoat samples were conducted on the B18 Core extended x-ray absorption fine structure (EXAFS) beamline at the Diamond Light Source, UK [31]. The measurements were carried out using a Si 311 double crystal monochromator. The spectra were collected in fluorescence mode using a 36 element Ge detector system, which was placed perpendicular to the incoming beam on the sample. The size of the beam used at the sample was approximately 200 (H) × 250 (V) μm. The Pd *K*-edge spectra were obtained to a *k*-space<sub>max</sub> 10.7 Å<sup>-1</sup>, with a time resolution of 180 s. Under isothermal conditions, 10 Pd scans were merged per temperature point.

The capillary flow microreactor was custom designed at B18 Diamond Light Source as shown in figure 1. The reactor was constructed out of ceramic, with a steel mounting rail to which a quartz capillary could be attached. Quartz capillaries (2.5 mm inner diameter) were packed with the catalysts and plugged with quartz wool. These capillaries were then mounted onto a steel rail and held using adhesive. Gas lines were fitted to the inlet and outlet of the capillary using Swagelok fittings, a *K*-type thermocouple was inserted through the outlet side of the capillary and was positioned in the middle of the catalyst bed. A secondary *K*-type thermocouple was used to control the temperature of the furnace. Mass spectrometry data of the outlet gases were collected using a Pfeiffer Omnistar GSD301 C mass spectrometer.

Approximately 65 mg of each sample, sieved to a particle size range of 250–125 μm, were loaded into the quartz capillary, giving a bed length of 12 mm, corresponding to a gas hourly space velocity of 102 715 h<sup>-1</sup>. Room temperature Pd *K*-edge XAFS were acquired while the sample was under a flow of He (100 ml min<sup>-1</sup>). The samples were heated under a reactive gas feed comprised of: CO<sub>2</sub> (2%), CO (0.5%), O<sub>2</sub> (0.5%), NO (1000 ppm), C<sub>3</sub>H<sub>8</sub> (1000 ppm) and He (Balance), at a total flow rate of 100 ml min<sup>-1</sup>. The sample was heated at 10 °C min<sup>-1</sup>, during which Pd *K*-edge XAFS spectra were collected. The samples were stabilised at 5 different temperatures: 100 °C, 130 °C, 230 °C, 750 °C and 200 °C (upon cooldown from 1000 °C), at which time, and isothermal Pd *K*-edge



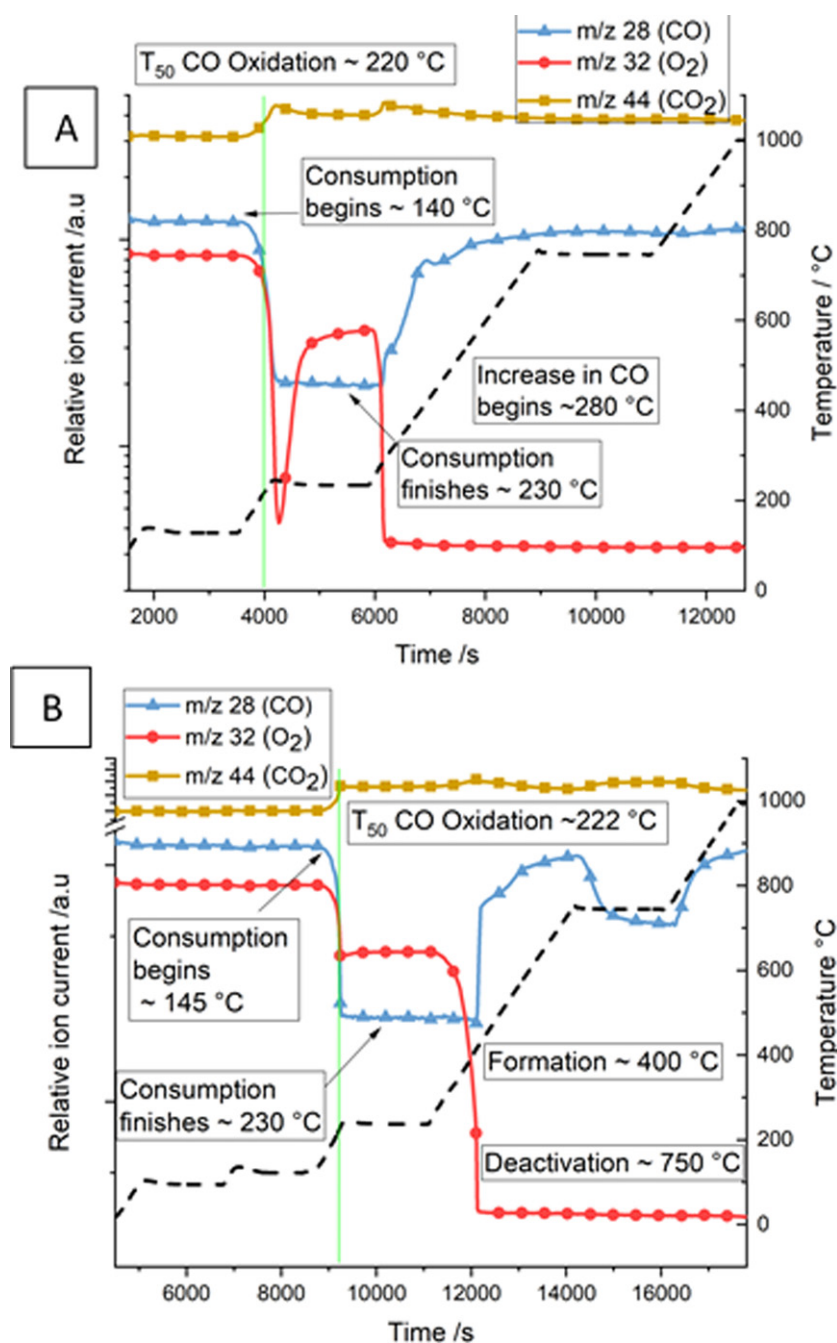


**Figure 2.** Mass Spectrometry profiles of fragments at 28 (CO), 32 (O<sub>2</sub>) and 44 (CO<sub>2</sub>) for washcoat sample (A) and 0 g ash GPF sample (B) on ramping at 10 °C min<sup>-1</sup> from room temperature to 1000 °C under a model exhaust gas feed conditions. The temperature profile is shown by the dashed line.

EXAFS were acquired. Pd *K*-edge XANES were also acquired during the ramp down to room temperature.

### 2.3. XAS analysis

The processing of EXAFS and XANES data was performed using IFEFFIT with the demeter package (Athena and Artemis) [32]. Reference foil spectra were acquired in transmission, using ion chamber detectors when no sample was in the beam.

The  $k^2$  weighted EXAFS data at an appropriate  $k$  range (up to 10.6 Å<sup>-1</sup>, and at most 9.4 independent points) was used.

Using a  $k$ -weighting of two provides an adequate scattering contribution between low  $Z$  value (O) and high  $Z$  value (Pd) species present [33, 34]. Fourier transformed data analysis was limited to the first shell scattering paths between Pd–Pd (2.734 Å) found in Pd foil, and the Pd–Pd (3.030 Å) as well as the Pd–O (2.018 Å) scattering paths found in bulk PdO. Spectra for PdO was acquired *ex situ* at the beamline prior to the experiment. The amplitude reduction factor,  $S_0^2$ , of 0.85 was determined from Pd *K*-edge EXAFS of Pd foil, by setting a fixed Pd–Pd coordination number of 12. Isothermal EXAFS measurements merged at least 10 spectra together in order to

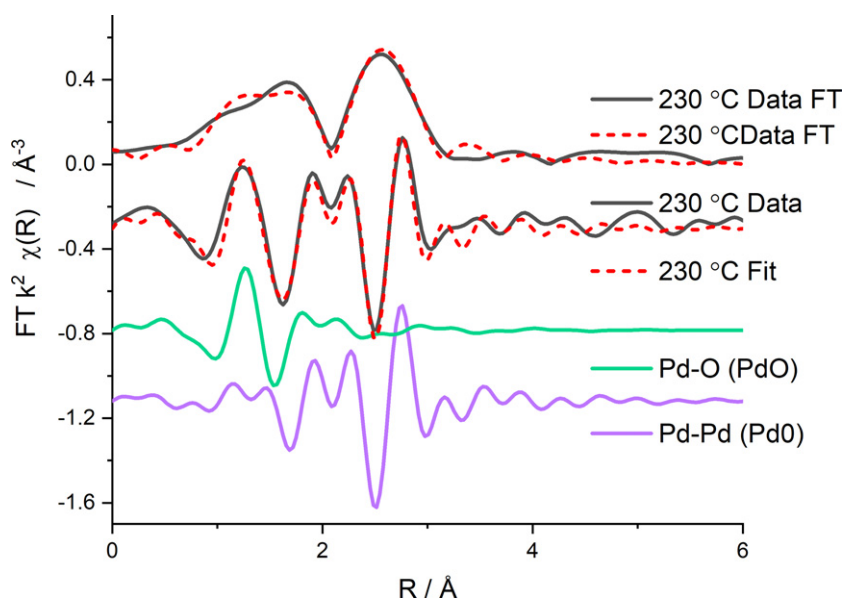


**Figure 3.** Magnitude of the  $k^2$ -weighted, FT of the experimental Pd K-edge EXAFS data for the washcoat close to the CO oxidation temperature of 230 °C. The imaginary components of the scattering paths of Pd–Pd of Pd<sup>0</sup> and the Pd–O consistent with PdO used in the fits.

**Table 1.** Pd K-edge EXAFS fitting parameters<sup>a</sup> for the washcoat and 20 g l<sup>-1</sup> ash-loaded samples at room temperature and at their respective CO light-off temperatures.

Conditions	Atom pair	$\Delta E_0$ (eV)	CN	$R$ (Å)	$\sigma^2$ (Å <sup>2</sup> )	$R_{\text{factor}}$
Washcoat at 20 °C	Pd–O	$-2 \pm 3$	$3.6 \pm 0.3$	$1.97 \pm 0.02$	0.0029	0.008
	Pd–Pd <sup>0</sup>		$0.4 \pm 0.3$	$2.67 \pm 0.05$	0.0019	
	Pd–Pd(PdO)		—	—	—	
Washcoat at 230 °C	Pd–O	$-5 \pm 3$	$1.3 \pm 0.4$	$1.96 \pm 0.04$	0.0042	0.03
	Pd–Pd <sup>0</sup>		$4.5 \pm 0.7$	$2.76 \pm 0.03$	0.0078	
	Pd–Pd(PdO)		—	—	—	
20 g l <sup>-1</sup> ash-loaded GPF at 20 °C	Pd–O	$1 \pm 3$	$3.6 \pm 0.4$	$2.02 \pm 0.02$	0.0013	0.03
	Pd–Pd(PdO)		$4 \pm 1$	$3.07 \pm 0.03$	0.0052	
20 g l <sup>-1</sup> ash-loaded GPF at 255 °C	Pd–O	$0 \pm 4$	$2.8 \pm 0.4$	$2.02 \pm 0.03$	0.0026	0.009
	Pd–Pd(PdO)		$3 \pm 2$	$3.02 \pm 0.06$	0.0066	
	Pd–Pd <sup>0</sup>		$2 \pm 2$	$2.78 \pm 0.06$	0.0072	

<sup>a</sup>Fitting parameters:  $S_0^2$  determined from Pd foil = 0.85,  $1 < R < 3.0$  Å,  $K$ -range 3.0–9.1, no. of independent points 7.56.

improve the signal to noise. Likewise, for the EXAFS acquired during temperature ramps, similar spectra within a temperature range of around 50 °C (at most 3) were merged.

### 3. Results and discussion

Here we investigate industrial GPF model catalysts. Firstly we study the effect of the manufacturing process on the catalyst activity evaluated through the comparison of the catalytic activity of the fresh washcoat with a sample extracted from a GPF with no ash deposition (0 g GPF). Secondly we study the effect of ash loading by comparing the 0 g GPF with the 20 g GPF.

#### 3.1. Effect of the GPF production

Comparing the mass spectrometry profiles under model exhaust conditions of the catalyst washcoat and the 0 g ash

GPF both show a similar CO oxidation light off temperature, the temperature at which 50% of the CO has been consumed ( $T_{50\text{CO}}$ ), was reached at 220 °C, figure 2.

The Pd K-edge EXAFS conducted on the washcoat system, suggests at room temperature that metallic Pd is present with an oxygen surface, with the data fitting well using a Pd–O scattering path at  $1.97 \pm 0.02$  Å and a Pd–Pd scattering path at  $2.67 \pm 0.05$  Å, consistent with Pd<sup>0</sup>. It was initially predicted that the Pd species would be more akin to PdO, though a reason for this initial difference in Pd speciation could be due to the manufacturing process of GPFs, where the catalyst washcoat undergoes high calcination temperatures to adhere onto the monolith channel walls and allow for decomposition of metal precursor compounds. During CO oxidation an increase in metallic Pd contribution was observed, figure 3, which shows the non phase-corrected Fourier transform of the  $k^2$  weighted Pd K-edge EXAFS data (plus imaginary components of the data, fit and scattering paths) of the washcoat sample recorded close to CO light-off temperature. The data can be fitted well using

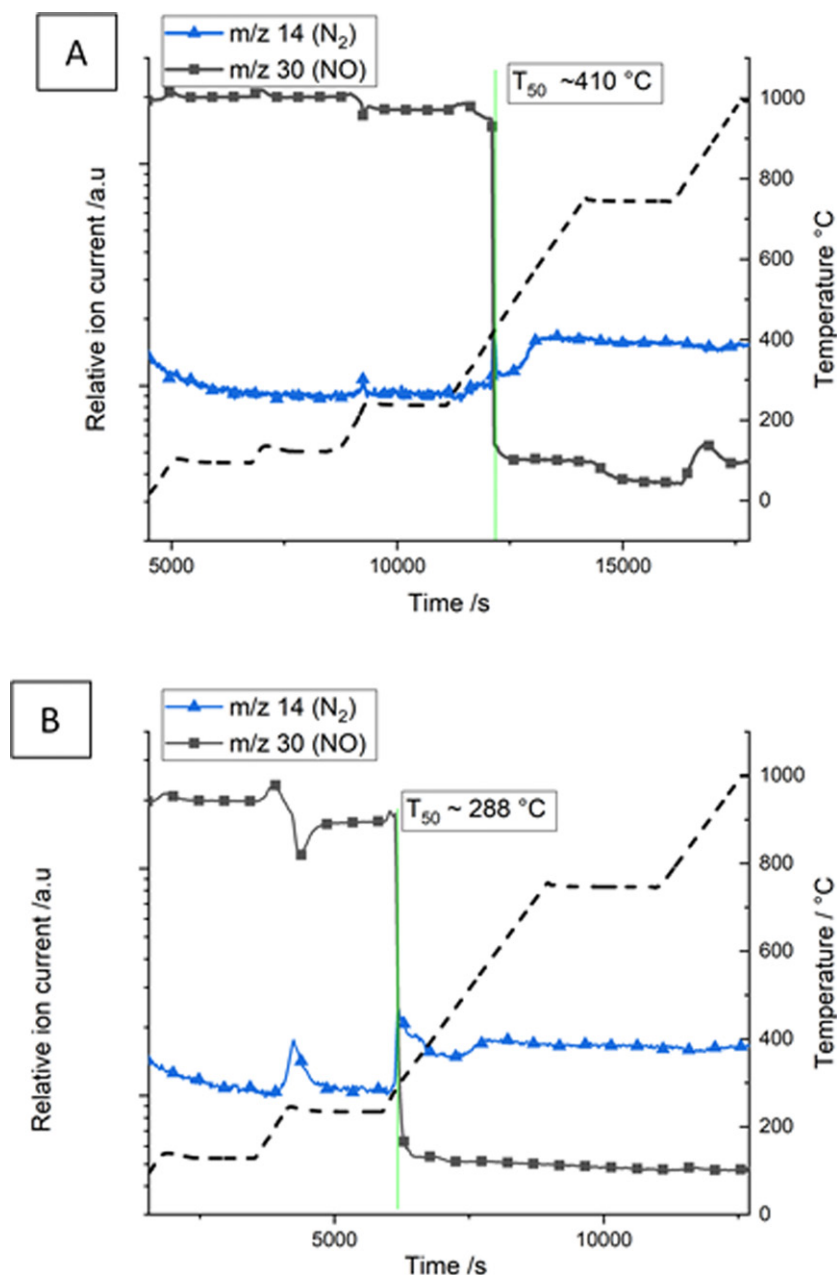


**Figure 4.** Mass Spectrometry profiles of NO consumption and N<sub>2</sub> formation of the 0 g GPF sample (A) and the washcoat sample (B) on ramping at 10 °C min<sup>-1</sup> from room temperature to 1000 °C under a model exhaust gas feed conditions. The temperature profile is shown by the dashed line.

two scattering paths, a Pd–Pd scattering path of 2.75 Å consistent with Pd<sup>0</sup> and the Pd–O scattering path. The coordination number of the metal contribution increases from 0.4 at room temperature to 4.5 during CO light-off, table 1. Likewise, the EXAFS analysis also indicated that the Pd species within the washcoat undergo reduction, with the O coordination number reducing from 3.6 to 1.3.

On increasing temperature, a sharp onset of NO consumption is observed coincident with the formation of N<sub>2</sub>, consistent with NO reduction, as shown in the mass spectrometry data in figure 4. A significantly higher NO reduction temperature was observed over the 0 g GPF catalyst, with a  $T_{50\text{ NO}}$  of 410 °C compared to a  $T_{50\text{ NO}}$  of 288 °C

for the washcoat sample, as shown in figures 4(A) and (B), respectively. Interestingly, on cooling, post high temperature ageing, both the washcoat sample, and the 0 g GPF sample had comparable NO light off temperatures of 310 °C, shown in figure S1 (see supporting information (<https://stacks.iop.org/JPCM/33/284001/mmedia>)). Surprisingly, the high temperature ageing process appears to be advantageous in the case of NO reduction.

From the Fourier Transform of the  $k^2$  weighted EXAFS data taken close to the NO light off temperature, a slight increase in the Pd<sup>0</sup> contribution to the EXAFS is observed along with the continued presence of a small contribution of Pd–O scattering. (Figure 5, table 2). The rise in the presence of metallic Pd was

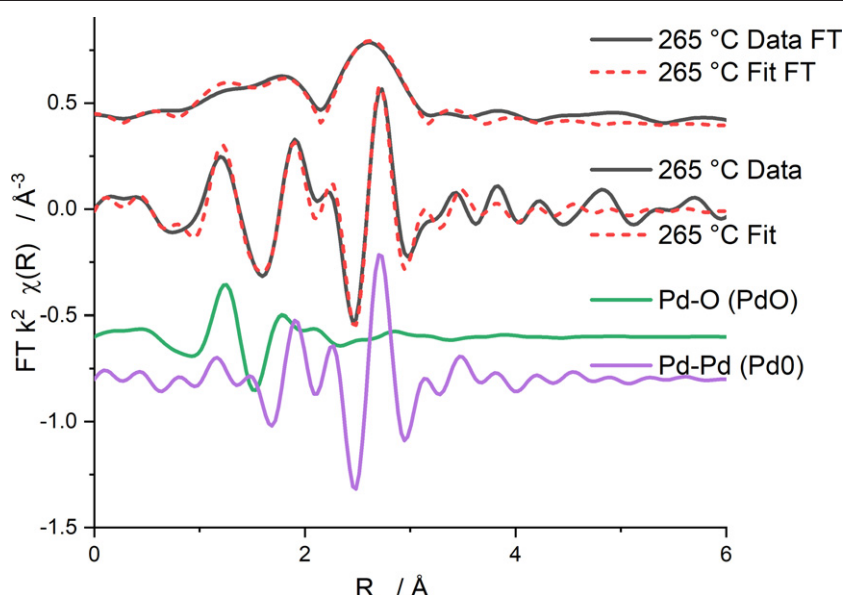


**Figure 5.** Magnitude of the  $k^2$ -weighted Fourier transform of the Pd  $K$ -edge EXAFS data for the washcoat sample around the NO light off temperature of 265 °C. The imaginary components of the scattering paths of Pd–Pd of Pd<sup>0</sup> and the Pd–O consistent with PdO used in the fits.

**Table 2.** Pd  $K$ -edge EXAFS fitting parameters<sup>a</sup> for the washcoat and 20 g ash-loaded samples at room temperature and their respective NO light-off temperatures of 265 and 382 °C.

Conditions	Atom pair	$\Delta E_0$ (eV)	CN	$R$ (Å)	$\sigma^2$ (Å <sup>2</sup> )	$R_{\text{factor}}$
Washcoat at ~265 °C	Pd–O	$-1 \pm 2$	$1.2 \pm 0.4$	$1.95 \pm 0.03$	0.0053	0.036
	Pd–Pd	—	—	—	—	
	Pd–Pd <sup>0</sup>	—	$5.1 \pm 0.7$	$2.77 \pm 0.01$	0.0085	
20 g l <sup>-1</sup> ash-loaded GPF at ~382 °C	Pd–O	$0 \pm 4$	$2.3 \pm 0.2$	$2.02 \pm 0.02$	0.0025	0.02
	Pd–Pd (PdO)	—	$2.1 \pm 0.6$	$3.02 \pm 0.03$	0.0042	
	Pd–Pd <sup>0</sup>	—	$1.6 \pm 0.6$	$2.78 \pm 0.03$	0.0050	

<sup>a</sup>Fitting parameters:  $S_0^2$  determined from Pd foil = 0.85,  $1 < R < 4.0$  Å,  $K$ -range 3.0–9.1, no. of independent points 7.56.

observed to begin from room temperature, reaching a maximum at ~350 °C. After cooling, this sample appeared to be more metallic in nature compared to the sample at room temperature as the scattering path for Pd–O or Pd–Pd from PdO were no longer required in the EXAFS fits, where the pattern was associated uniquely to a Pd–Pd scattering path from Pd<sup>0</sup> (see table S1 of supporting information).

The mass spectrometry data in figure 6(A) shows that full propane consumption was observed at a  $T_{50\text{C}_3\text{H}_8}$  of 325 °C for the washcoat sample. At this temperature the EXAFS data suggests that the Pd was metallic, table 3, figure 7, with minimal contribution of a Pd–O scattering path, as shown from the imaginary components of the scattering paths in figure 7, the EXAFS are dominated by the metal scattering path. The 0 g ash GPF sample has a much higher propane consumption temperature of 410 °C. In both cases, during propane consumption an increase in the mass fragments associated with hydrogen ( $m/z$  2), water ( $m/z$  18), ethylene ( $m/z$  26), and carbon monoxide ( $m/z$  28) were observed with a slight fall in carbon dioxide ( $m/z$  44), which may suggest a competition between the processes of complete propane oxidation (forming CO<sub>2</sub>), propane dehydrogenation and subsequent propene

cracking to form ethylene and methane, (figure S3 and S4 of supporting information). These cracking and dehydrogenation products were also observed during the blank experiment with no catalyst, but at a very low proportion and at significantly higher temperatures (500–700 °C), figure S2, implying that while some part is attributed to thermal effects, the catalyst is facilitating this hydrocarbon conversion pathway.

Summarising the observed changes in Pd speciation of the washcoat sample during the *operando* XAFS study: firstly, at high temperatures (>800 °C) the system shows a significant presence of Pd<sup>0</sup>, with a CN of around ~10. Interestingly, an apparent phase hysteresis in Pd oxidation state was also observed between 450 °C and 730 °C, where the sample was initially mostly metallic Pd; this contribution then decreased while the amount of PdO increased; above 730 °C the system reverted to an exclusively metallic Pd.

### 3.2. Effect of ash loading

At room temperature, for the 20 g ash GPF sample, the Pd  $K$ -edge EXAFS data are consistent with PdO, with the EXAFS data fitting well to a Pd–O scattering path of  $2.02 \pm 0.02$  Å



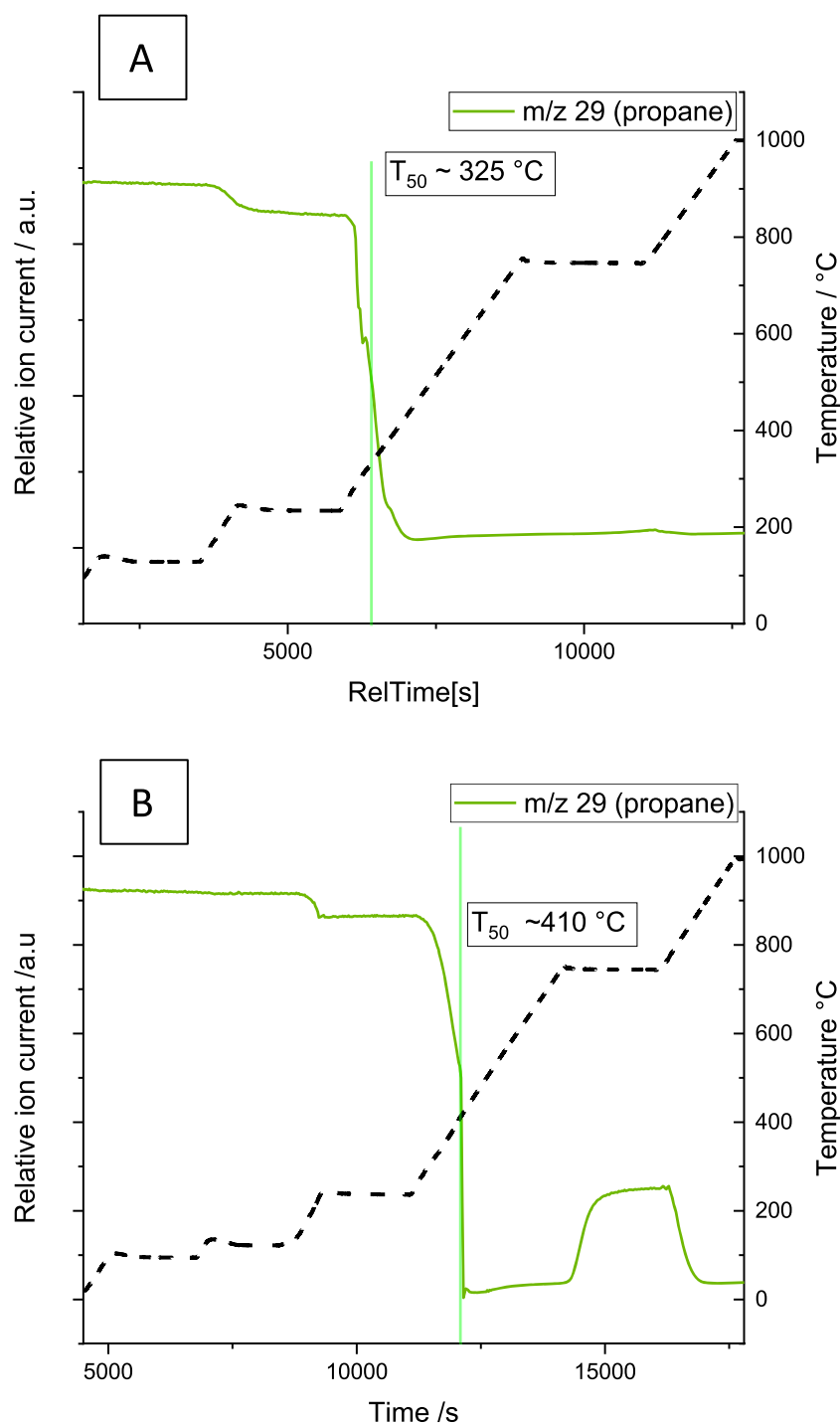


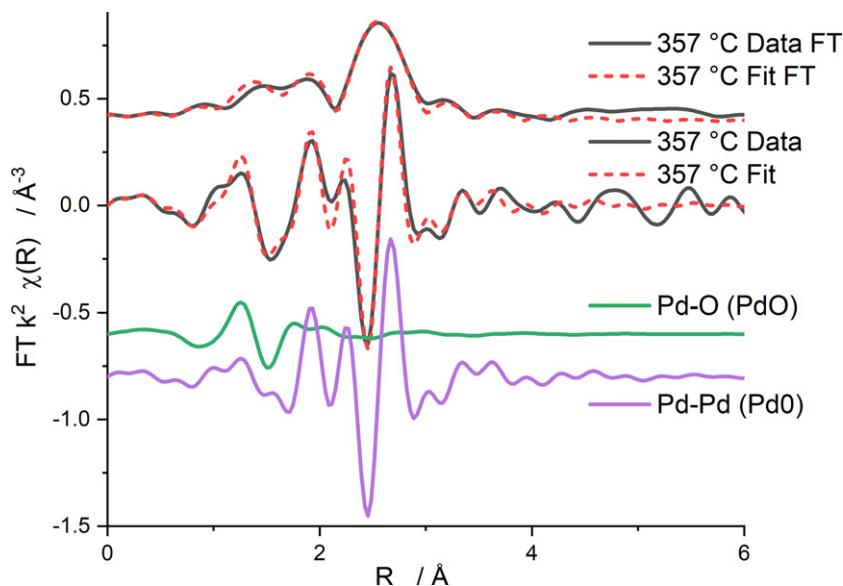
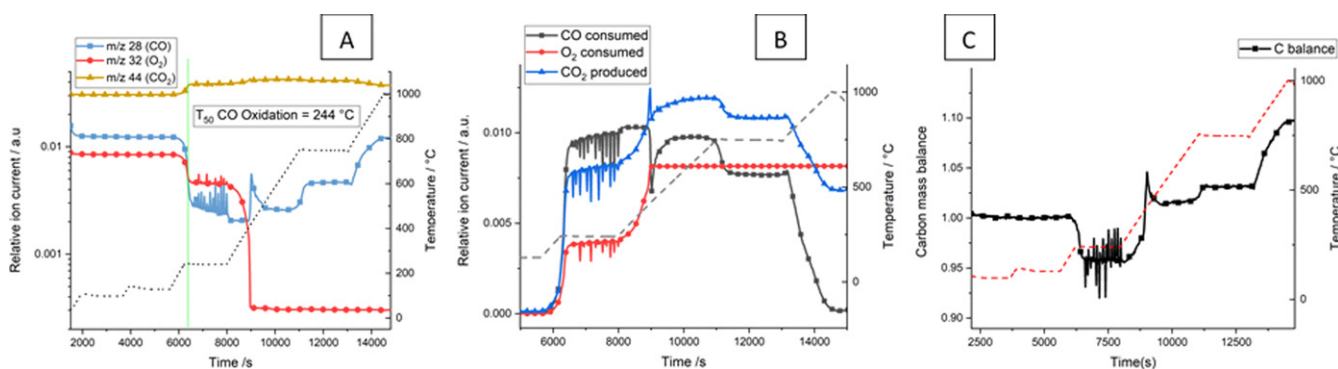
**Figure 6.** Mass spectrometry profiles of propane consumption of the washcoat sample (A) and the 0 g ash GPF sample (B) on ramping at  $10$  °C  $\text{min}^{-1}$  from room temperature to  $1000$  °C under model exhaust gas feed conditions.

and a Pd–Pd scattering path of around  $3.06 \pm 0.02$  Å, consistent with PdO. This difference in Pd speciation compared to the washcoat sample, which was metallic Pd NPs at room temperature, could be due to the high temperature treatment used to add the catalyst to the GPF or also the ash deposition treatment, as outlined in the Experimental section. As the reaction proceeded, a higher CO oxidation  $T_{50\text{CO}}$  was observed for the sample from the 20 g ash GPF compared with the 0 g ash GPF, at  $242$  °C and  $220$  °C respectively, as shown in figure 8

and figure 2(B). Oscillations in the CO and CO<sub>2</sub> mass spectrometer responses ( $m/z$  28 and 44) were observed during CO oxidation for the 20 g ash GPF sample. Dann *et al* observed a similar oscillation pattern with Pd/ $\gamma$ -Al<sub>2</sub>O<sub>3</sub> where the oscillations were attributed to the competition of CO storage and formation of a surface oxide on the surface of the nanoparticle [34]. Here, taking the ratio of CO<sub>2</sub> produced to O<sub>2</sub> consumed from figure 2(B) the value oscillates around 2, the stoichiometry consistent with CO oxidation. However, the ratio of CO<sub>2</sub>

**Table 3.** Pd K-edge EXAFS fitting parameters<sup>c</sup> for the washcoat and 20 g ash-loaded sample at room temperature and their respective propane light-off temperatures.

Conditions	Atom pair	$\Delta E_0$ (eV)	CN	$R$ (Å)	$\sigma^2$ (Å <sup>2</sup> )	$R_{\text{factor}}$
Washcoat at 357 °C <sup>b</sup>	Pd–O	$-2 \pm 2$	$0.7 \pm 0.4$	$1.95 \pm 0.04$	0.0057	0.07
	Pd–Pd	—	—	—	—	
	Pd–Pd <sup>0</sup>	—	$5.4 \pm 0.8$	$2.75 \pm 0.02$	0.0096	
20 g l <sup>-1</sup> ash-loaded GPF at 472 °C	Pd–O	$-1 \pm 2$	$2.7 \pm 0.2$	$2.02 \pm 0.02$	0.0026	0.026
	Pd–Pd	—	$1.6 \pm 0.8$	$3.00 \pm 0.04$	0.0053	
	Pd–Pd <sup>0</sup>	—	$1.3 \pm 0.8$	$2.77 \pm 0.04$	0.0070	

<sup>a</sup>K-range 3.1–8.8, no. of independent points 7.06.<sup>b</sup>K-range 3.1–10.0, no. of independent points 8.56.<sup>c</sup>Fitting parameters:  $S_0^2$  determined from Pd foil = 0.85,  $1 < R < 3.0$  Å.**Figure 7.** Magnitude of the  $k^2$ -weighted Fourier transform of the Pd K-edge EXAFS data for the washcoat sample around the propane light off temperature of 357 °C. The imaginary components of the scattering paths of Pd–Pd of Pd<sup>0</sup> and the Pd–O used in the fits.**Figure 8.** Mass spectrometry profile of fragments at  $m/z$  28 (CO),  $m/z$  32 ( $O_2$ ) and  $m/z$  44 ( $CO_2$ ) for and 20 g ash GPF sample (A). The CO and  $O_2$  consumed and  $CO_2$  produced are shown in (B) and the carbon mass balance (C) for the 20 g ash GPF reaction up to 1000 °C, where carbon balance is the sum of the  $CO_2$ , CO and propane divided by the value at 4000s, prior to the onset of reaction.

produced to CO consumed is always  $< 1$ , implying some possible competition for CO consumption which does not have a 1:1 stoichiometry with  $CO_2$  or some additional production of CO.

We speculate that there are three reactions contributing to these oscillations, CO oxidation, C deposition, possibly via

the Boudouard reaction and partial oxidation of the carbon to produce primarily CO, as oxygen supply is limited. This production of CO would help to explain the sharp drops in CO consumption which do not always coincide with  $CO_2$  production. The carbon mass balance, figure 8(C), shows that, during the region of these oscillations, some carbon deposition occurs.

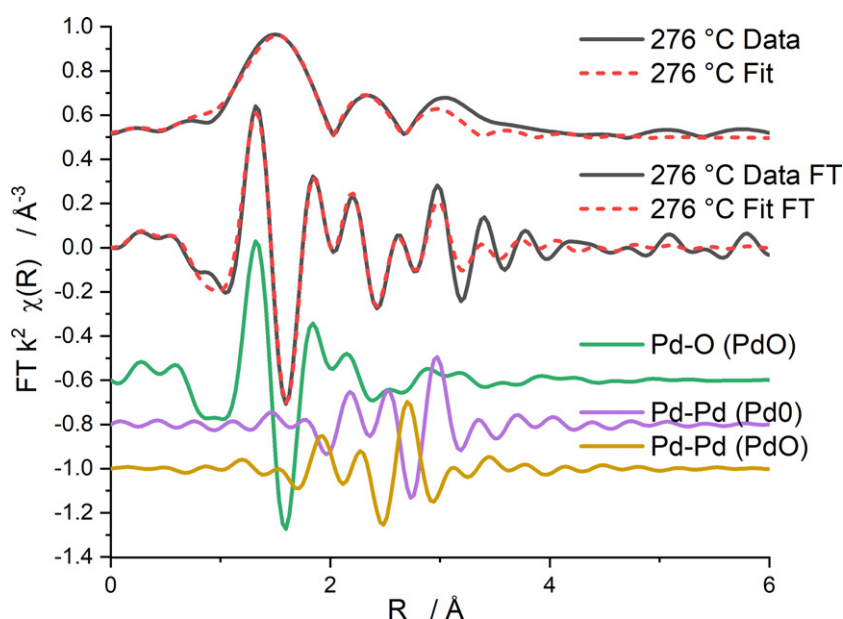


**Figure 9.** Magnitude of the  $k^2$ -weighted, FT of the experimental Pd  $K$ -edge EXAFS data for the 20 g ash GPF system around the CO light off temperature of 276 °C. The imaginary components of the 3 scattering paths used in the fit are shown.

The oscillation process was not observed from the MS profile of the catalyst from the 0 g ash GPF, which suggest that this could be due to the addition of the ash components present in the system.

From the Pd  $K$ -edge EXAFS analysis, an increase in metallic Pd contribution was observed during CO oxidation. A Pd–Pd scattering path of 2.75 Å consistent with Pd<sup>0</sup> was required to fit the data, with coordination numbers increasing from 0 to 2 from room temperature to the CO light-off temperature range, table 1. A slight reduction in O coordination number was also observed, reducing from 3.8 to 2.8. However, some evidence of remaining PdO was observed through the continued presence of the Pd–Pd scattering path around 3 Å, figure 9.

A similar NO reduction temperature (figure 10 and figure 4) was also observed for both the 20 g ash GPF sample and the 0 g ash GPF samples, with a  $T_{50\text{NO}}$  of around 410 °C. However, on cooling, post high temperature ageing, the 0 g ash GPF sample had an NO light-off temperature of 310 °C whereas the 20 g ash GPF sample maintained its high temperature NO light-off of 410 °C, figure S1 (see supporting information). It would appear that the combination of ash and ageing leads to an irreversible increase in NO reduction temperature. During the ageing process, at NO light-off temperatures, the Pd speciation did show significant change from that observed during CO light off with Pd–Pd scattering paths from both PdO and Pd<sup>0</sup> present, table 2 and figure 11. After cooling, the sample is fully metallic in nature compared to the fresh sample, as the scattering path for Pd–O or Pd–Pd from PdO were no longer present in the EXAFS fits, the data was fitted uniquely to a Pd–Pd scattering path from Pd<sup>0</sup>. Table S3 (see supporting information).

The  $T_{50}$  for propane ( $T_{50\text{C}_3\text{H}_8}$ ) consumption occurred around 410 °C in both the 0 g ash and 20 g ash GPF

samples, figure 6 and 12. At this temperature the 20 g ash GPF sample has a contribution from PdO still present in the EXAFS data, figure 13. From the mass spectrometry profile, figure 12, the 20 g ash GPF sample showed a more gradual decrease in the propane mass fraction until 750 °C when the majority of the propane was then converted into ethylene and methane. Between 375 °C and 475 °C an increase in the mass fragments associated with hydrogen ( $m/z$  2), water ( $m/z$  18), ethylene ( $m/z$  26), and carbon monoxide ( $m/z$  28) were observed with a slight fall in carbon dioxide ( $m/z$  44), which may suggest a competition between the processes of complete propane oxidation (forming CO<sub>2</sub>), propane dehydrogenation and subsequent propene cracking to form ethylene and methane (figure S5 of supporting information). However, as explained earlier the conversion at high temperature was associated to a thermal effect. It should be noted that the formation of methane and ethylene was observed to be more prominent in the ash loaded system compared to the 0 g GPF sample (see supporting information S2).

On increasing temperature (>800 °C) during the ageing process, the 20 g ash GPF sample shows a significant presence of Pd<sup>0</sup>, with a CN of around 10, table S4. However, an additional complication in the EXAFS fitting was observed in this sample from 680 °C–850 °C. The EXAFS analysis suggested that a Pd scattering path of 2.9 Å which could not be associated with Pd scattering from PdO (3.02 Å) or Pd<sup>0</sup> (2.75 Å), was required to fit the data. It was initially postulated that this could be an association of Pd migrating into a vacant sites in CeO<sub>2</sub>, as this is present within the oxide support; however this distance would have been too large (cerium to oxygen distance being around 2.3 Å). Likewise, the incorporation into other vacant sites within the support including the alumina would have been too large [35]. The suggestion of the formation of

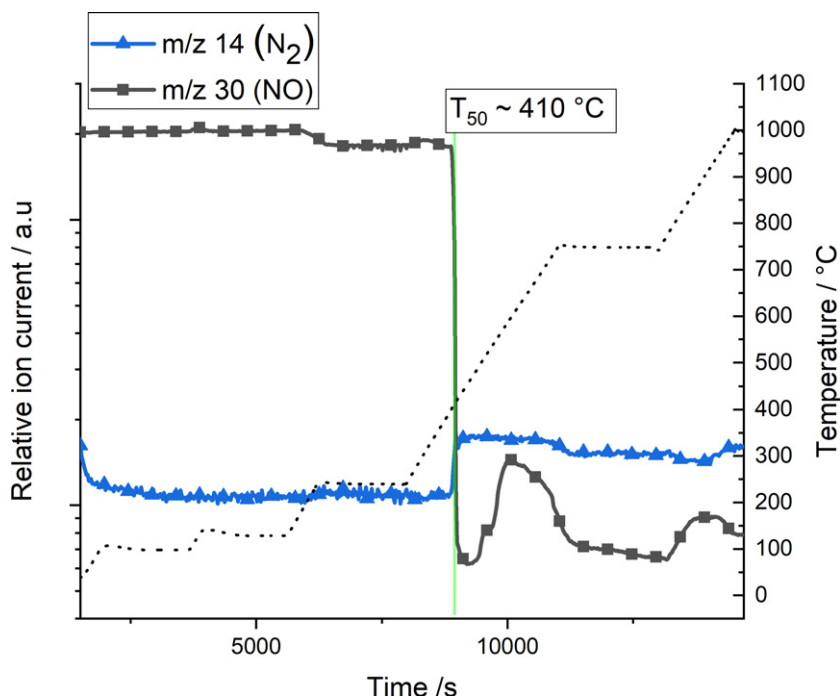


**Figure 10.** Mass spectrometry profiles of NO consumption and N<sub>2</sub> formation of the 20 g ash GPF sample on ramping at 10 °C min<sup>-1</sup> from room temperature to 1000 °C under model exhaust gas feed conditions.

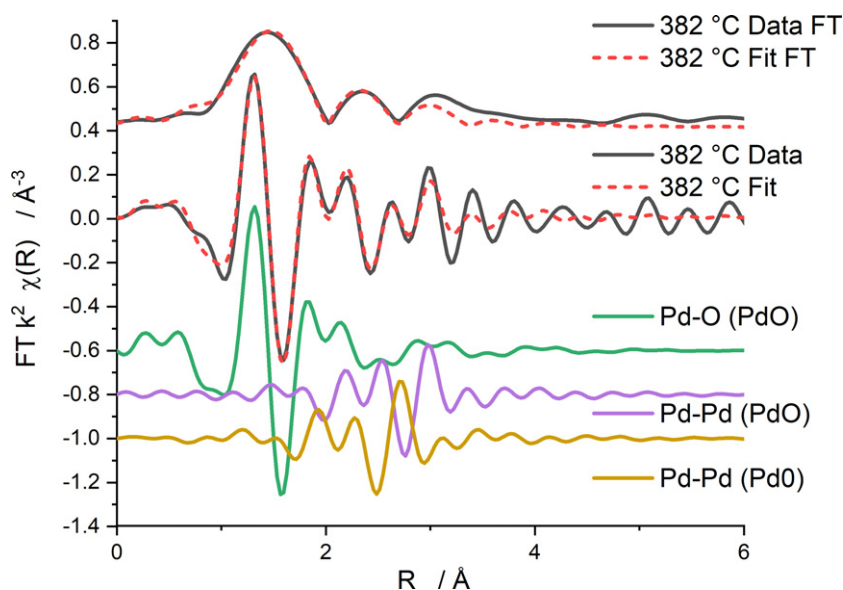


**Figure 11.** Magnitude of the  $k^2$ -weighted Fourier transform of the Pd  $K$ -edge EXAFS data for the 20 g ash GPF sample around the NO light off temperature of 362 °C. The imaginary components of the 3 scattering paths used in the fit are shown.

an interstitial carbide or hydride was also explored for these systems. Observing the white line intensity within the XANES and shifts in the reciprocal space in the EXAFS, implied that there was a low probability of interstitial carbide formation. This observation is in agreement with the work of Bugaev *et al*: the presence of a carbide species on Pd would be distinguishable by the negligible change in the white line intensity when compared to the metallic species, alongside a shift to lower radial distances when comparing the oscillations in reciprocal space [36]. Although a Pd hydride may be a likely candidate

due to the production of hydrogen prior to the appearance of this EXAFS feature and fitting a Pd to Pd scattering path at 2.89 Å associated with PdH could be used to model the spectra obtained at this temperature range (see table S1) [37]. However, the associated XANES features with a PdH<sub>x</sub>, as described by Bugaev *et al*, a slight shift in the energy of the white line feature when compared to Pd metal and a positive difference when subtracting the spectra to the reference foil, are not observed. Another possibility is that a phase change of Pd metal could occur under these conditions. However, a recent



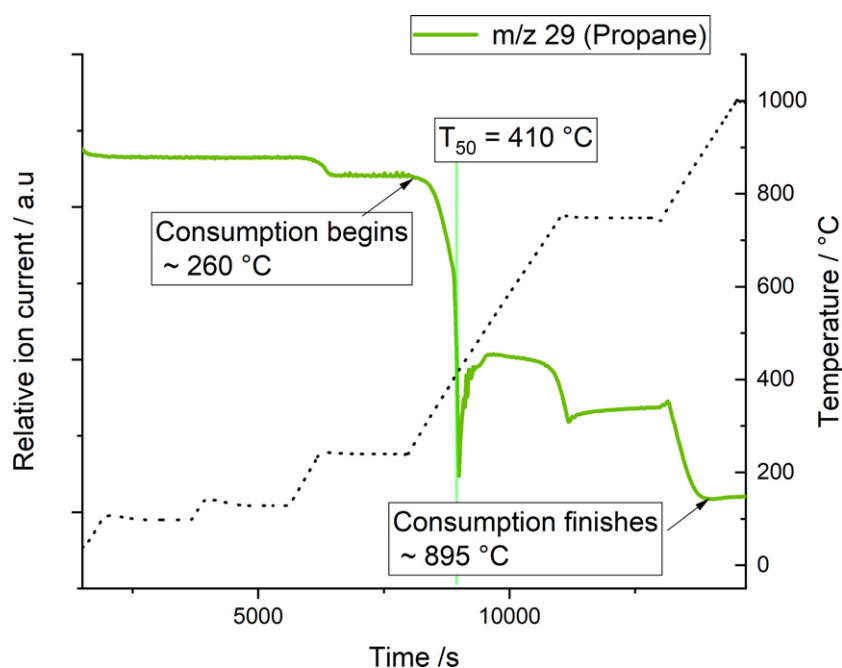


**Figure 12.** Mass spectrometry profiles of propane consumption of the 20 g ash GPF sample on ramping at  $10\text{ }^{\circ}\text{C min}^{-1}$  from room temperature to  $1000\text{ }^{\circ}\text{C}$  under model exhaust gas feed conditions.

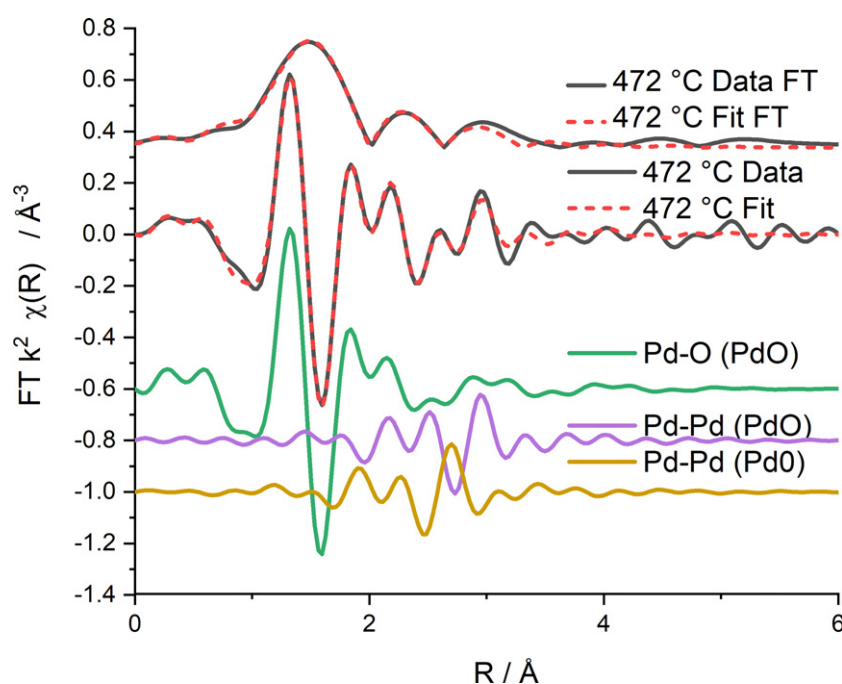


**Figure 13.** Magnitude of the  $k^2$ -weighted Fourier Transform of the Pd  $K$ -edge EXAFS data for the 20 g ash loaded sample near the propane light off temperature of  $472\text{ }^{\circ}\text{C}$ . The imaginary components of the 3 scattering paths used in the fit are shown.

computational study based on density functional theory suggests that the Pd–Pd bond distance in the hcp phase would be  $2.76\text{ }\text{\AA}$  at room temperature. [38] After around  $900\text{ }^{\circ}\text{C}$ , the species begins to reduce and a phase more akin to metallic Pd begins to form, as shown in table S4. Having ruled out

numerous potential Pd structures, it is possible that at these temperatures the Pd is a mixture of metal and oxide resulting in an intermediate Pd–Pd distance as determined from the EXAFS analysis. These small mixed oxide and metallic particles may be stabilised by the support but on increasing

temperature are reduced fully. It should be noted it is not the first time these intermediate Pd distances have been observed over Pd/Al<sub>2</sub>O<sub>3</sub> catalysts at similar temperatures [39].

#### 4. Summary and conclusion

An *operando* XAFS investigation was performed on two model catalysts used in three-way catalysis within GPFs, with the aim to understand both the effect that the production of GPFs has on the performance of the catalyst and the role that ash plays in the catalytic activity. To achieve this *operando* XAFS was conducted on one sample from a catalyst washcoat which had not been previously adhered onto a GPF monolith and the other was extracted from a GPF with 20 g l<sup>-1</sup> of ash pre-deposited onto the system. Both activity profiles were compared to what was observed with a catalyst extracted from a GPF containing no-ash components (0 g ash GPF). This XAFS study under model gas mixture conditions representative of exhaust gases showed that within the washcoat sample a hysteresis of oxidation state of the Pd is observed in the washcoat sample. Furthermore, an increase in metallic Pd was observed during CO oxidation. Oscillations in the CO, O<sub>2</sub> and CO<sub>2</sub> signals were observed in the 20 g ash GPF sample and are speculatively associated with a combination of CO oxidation, C deposition possibly via the Boudouard reaction and partial oxidation to CO of the deposited C, which is suggested to be facilitated by the presence of calcium in the ash. The washcoat sample appears to have a lower light-off temperature for NO reduction compared to the 0 g ash GPF sample implying that the necessary process of adhering the catalyst onto the GPF may adversely affect the catalyst's ease of NO reduction. However, comparing the NO reduction temperature post high temperature ageing of the 0 g and 20 g ash GPF samples, the 0 g ash GPF sample recovers and has NO light-off similar to that of the washcoat (310 °C), whereas the combined effect of ash and ageing results in a high temperature NO reduction temperature, (410 °C). Assuming the 0 g ash GPF and washcoat samples must be similar post ageing due to the similar *T*<sub>50 NO</sub> temperatures, comparison of the XAFS data of the washcoat and 20 g ash GPF sample would be expected to provide some indication of the structural differences responsible. However, on comparison of the XAFS data of the washcoat and 20 g ash GPF samples post ageing, both appear to be fully metallic by this point. Future studies will be reported in order to understand this interesting observation.

#### Acknowledgments

The authors would like to thank Diamond Light Source for provision of beamtime SP24156, the UK Catalysis Hub access to equipment and the EPSRC (EP/R512138/1) for the iCASE studentship for M Panchal. Johnson Matthey is thanked for the studentship and providing the GPF materials for Monik Panchal. Lara Kabalan is thanked for communicating the results of DFT calculations prior to publication. Donato Decarolis is thanked for his insight and consultation with MS analysis. Support from the UK Catalysis Hub (EP/R026939/1,

EP/R026815/1) is gratefully acknowledged. Stephan A Parry is thanked for the production of the B18 microreactor and Vladimír Novák is thanked for initial insight into the project and supplying the material from Johnson Matthey.

#### Data availability statement

All data that support the findings of this study can be accessed from the University of Glasgow's data repository: <http://dx.doi.org/10.5525/gla.researchdata.1141>.

#### ORCID iDs

Monik Panchal  <https://orcid.org/0000-0002-5218-7132>  
 June Callison  <https://orcid.org/0000-0003-4506-1862>  
 Vainius Skukauskas  <https://orcid.org/0000-0001-6858-4506>  
 Diego Gianolio  <https://orcid.org/0000-0002-0708-4492>  
 Giannantonio Cibi  <https://orcid.org/0000-0001-5761-6760>  
 Andrew P E York  <https://orcid.org/0000-0001-5857-7089>  
 Manfred E Schuster  <https://orcid.org/0000-0003-3399-7372>  
 Timothy I Hyde  <https://orcid.org/0000-0003-0435-2380>  
 C Richard A Catlow  <https://orcid.org/0000-0002-1341-1541>  
 Emma K Gibson  <https://orcid.org/0000-0002-7839-3786>

#### References

- [1] Banister D 2002 *Transport, Development and Sustainability* (London, UK: Spon Press)
- [2] Rezvani Z, Jansson J and Bodin J 2015 Advances in consumer electric vehicle adoption research: a review and research agenda *Transp. Res. D* **34** 122–36
- [3] Mukherjee S C and Ryan L 2020 Factors influencing early battery electric vehicle adoption in Ireland *Renew. Sustain. Energy Rev.* **118** 109504
- [4] Anjos M F, Gendron B and Joyce-Moniz M 2020 Increasing electric vehicle adoption through the optimal deployment of fast-charging stations for local and long-distance travel *Eur. J. Oper. Res.* **285** 263–78
- [5] Küfeoglu S and Khah Kok Hong D 2020 Emissions performance of electric vehicles: a case study from the United Kingdom *Appl. Energy* **260** 114241
- [6] Zelenka P, Cartellieri W and Herzog P 1996 Worldwide diesel emission standards, current experiences and future needs *Appl. Catal. B* **10** 3–28
- [7] Gerard D and Lave L B 2005 Implementing technology-forcing policies: the 1970 clean air act amendments and the introduction of advanced automotive emissions controls in the United States *Technol. Forecast. Soc. Change* **72** 761–78
- [8] Winkler S L, Anderson J E, Garza L, Ruona W C, Vogt R and Wallington T J 2018 Vehicle criteria pollutant (PM, NO<sub>x</sub>, CO, HCs) emissions: how low should we go? *npj Clim. At. Sci.* **1** 1–5
- [9] Su J, Lin W, Sterniak J, Xu M and Bohac S V 2014 Particulate matter emission comparison of spark ignition direct injection (SIDI) and port fuel injection (PFI) operation of a boosted gasoline engine *J. Eng. Gas Turbines Power* **136** 091513

- [10] Collings N and Graskow B R 2000 Particles from internal combustion engines—what we need to know *Phil. Trans. R. Soc. A* **358** 2611–23
- [11] Anon 2020 record year for zero emission cars fails to reboot UK market, as sector calls for supportive policies to boost uptake SMMT
- [12] Saliba G *et al* 2017 Comparison of gasoline direct-injection (GDI) and port fuel injection (PFI) vehicle emissions: emission certification standards, cold-start, secondary organic aerosol formation potential, and potential climate impacts *Environ. Sci. Technol.* **51** 6542–52
- [13] Awad O I, Ma X, Kamil M, Ali O M, Zhang Z and Shuai S 2020 Particulate emissions from gasoline direct injection engines: a review of how current emission regulations are being met by automobile manufacturers *Sci. Total Environ.* **718** 137302
- [14] Kurt O K, Zhang J and Pinkerton K E 2016 Pulmonary health effects of air pollution *Curr. Opin. Pulmon. Med.* **22** 138–43
- [15] Zhang R, Wang G, Guo S, Zamora M L, Ying Q, Lin Y, Wang W, Hu M and Wang Y 2015 formation of urban fine particulate matter *Chem. Rev.* **115** 3803–55
- [16] Anon 9 out of 10 people worldwide breathe polluted air, but more countries are taking action
- [17] Kleeman M J, Riddle S G, Robert M A and Jakober C A 2008 Lubricating oil and fuel contributions to particulate matter emissions from light-duty gasoline and heavy-duty diesel vehicles *Environ. Sci. Technol.* **42** 235–42
- [18] Liati A, Schreiber D, Dimopoulos Eggenschwiler P and Arroyo Rojas Dasilva Y 2013 Metal particle emissions in the exhaust stream of diesel engines: an electron microscope study *Environ. Sci. Technol.* **47** 14495–501
- [19] Liati A, Spiteri A, Dimopoulos Eggenschwiler P and Vogel-Schäuble N 2012 Microscopic investigation of soot and ash particulate matter derived from biofuel and diesel: implications for the reactivity of soot *J. Nanopart. Res.* **14** 1224
- [20] Spikes H 2008 Low- and zero-sulphated ash, phosphorus and sulphur anti-wear additives for engine oils *Lubrication Sci.* **20** 103–36
- [21] Sappok A, Santiago M, Vianna T and Wong V W 2009 *Characteristics and Effects of Ash Accumulation on Diesel Particulate Filter Performance: Rapidly Aged and Field Aged Results* (Warrendale, PA: SAE International)
- [22] Millet C-N, Chédotal R and Da Costa P 2009 Synthetic gas bench study of a four-way catalytic converter: catalytic oxidation, NO<sub>x</sub> storage/reduction and impact of soot loading and regeneration *Appl. Catal. B* **90** 339–46
- [23] Gill L J, Blakeman P G, Twigg M V and Walker A P 2004 The use of NO<sub>x</sub> adsorber catalysts on diesel engines *Top. Catal.* **28** 157–64
- [24] Sappok A G, Beauboeuf D and Wong V W 2008 A novel accelerated aging system to study lubricant additive effects on diesel after treatment system degradation *SAE Int. J. Fuels Lubr.* **1** 813–27
- [25] Shettigar V O and Pesiridis A 2014 Materials selection for variable geometry turbine nozzle for gasoline engine application *ASME Turbo Expo 2014: Turbine Technical Conf. and Exposition* (American Society of Mechanical Engineers Digital Collection)
- [26] Tojo M 2008 Development of compact and high performance turbocharger for 1 050 °C exhaust gas *Mitsubishi Heavy Industries Technical Review* **45** 1–5
- [27] Buwono H P, Eidome T, Minami S, Hinokuma S, Nagao Y, Nakahara Y and Machida M 2015 Rh supported on LaPO<sub>4</sub>/SiO<sub>2</sub> nanocomposites as thermally stable catalysts for TWC applications *Emiss. Control Sci. Technol.* **1** 284–91
- [28] Deganello F, Longo A and Martorana A 2003 EXAFS study of ceria-lanthana-based TWC promoters prepared by sol-gel routes *J. Solid State Chem.* **175** 289–98
- [29] Dann E K *et al* 2017 Combined in situ XAFS/DRIFTS studies of the evolution of nanoparticle structures from molecular precursors *Chem. Mater.* **29** 7515–23
- [30] Seong H, Choi S, Lee S, Zaluzec N J, Toops T J, Lance M J, Kim D and Nguyen K 2019 Deactivation of three-way catalysts coated within gasoline particulate filters by engine-oil-derived chemicals *Ind. Eng. Chem. Res.* **58** 10724–36
- [31] Dent A J *et al* 2013 Performance of B18, the Core EXAFS bending magnet beamline at Diamond *J. Phys.: Conf. Ser.* **430** 012023
- [32] Ravel B and Newville M 2005 ATHENA, ARTEMIS, HEPHAESTUS: data analysis for x-ray absorption spectroscopy using IFEFFIT *J. Synchrotron Radiat.* **12** 537–41
- [33] Koningsberger D C, Mojet B L, van Dorssen G E and Ramaker D E 2000 XAFS spectroscopy; fundamental principles and data analysis *Top. Catal.* **10** 143–55
- [34] Dann E K *et al* 2019 Combined spatially resolved operando spectroscopy: new insights into kinetic oscillations of CO oxidation on Pd/γ-Al<sub>2</sub>O<sub>3</sub> *J. Catal.* **373** 201–8
- [35] Wołczyr M and Kepinski L 1992 Rietveld refinement of the structure of CeOCl formed in Pd/CeO<sub>2</sub> catalyst: notes on the existence of a stabilized tetragonal phase of La<sub>2</sub>O<sub>3</sub> in LaPdO system *J. Solid State Chem.* **99** 409–13
- [36] Bugaev A L *et al* 2017 *In situ* formation of hydrides and carbides in palladium catalyst: when XANES is better than EXAFS and XRD *Catal. Today* **283** 119–26
- [37] Schirber J E and Morosin B 1975 Lattice constants of β-PdH<sub>x</sub> and β-PdD<sub>x</sub> with x near 1.0 *Phys. Rev. B* **12** 117–8
- [38] Kabalan L, Kowalec I, Lonsdail A J and Catlow C R A unpublished
- [39] Keating J, Sankar G, Hyde T I, Kohara S and Ohara K 2013 Elucidation of structure and nature of the PdO–Pd transformation using *in situ* PDF and XAS techniques *Phys. Chem. Chem. Phys.* **15** 8555–65